

# Semi-Supervised Wide-Angle Portraits Correction by Multi-Scale Transformer

Fushun Zhu<sup>1\*</sup>, Shan Zhao<sup>2\*</sup>, Peng Wang<sup>2\*</sup>, Hao Wang<sup>2</sup>, Hua Yan<sup>1</sup>, Shuaicheng Liu<sup>3,2†</sup>

<sup>1</sup> Sichuan University    <sup>2</sup> Megvii Research

<sup>3</sup> University of Electronic Science and Technology of China

{zhaoshan, wangpeng04, wanghao03}@megvii.com

zhufushun@stu.scu.edu.cn, yanhua@scu.edu.cn, liushuaicheng@uestc.edu.cn

## Abstract

We propose a semi-supervised network for wide-angle portraits correction. Wide-angle images often suffer from skew and distortion affected by perspective distortion, especially noticeable at the face regions. Previous deep learning based approaches require the ground-truth correction flow maps for the training guidance. However, such labels are expensive, which can only be obtained manually. In this work, we propose a semi-supervised scheme, which can consume unlabeled data in addition to the labeled data for improvements. Specifically, our semi-supervised scheme takes the advantages of the consistency mechanism, with several novel components such as direction and range consistency (DRC) and regression consistency (RC). Furthermore, our network, named as Multi-Scale Swin-Unet (MS-Unet), is built upon the multi-scale swin transformer block (MSTB), which can learn both local-scale and long-range semantic information effectively. In addition, we introduce a high-quality unlabeled dataset with rich scenarios for the training. Extensive experiments demonstrate that the proposed method is superior over the state-of-the-art methods and other representative baselines.

## 1 Introduction

The wide-angle camera, aiming to capture memorial moments filled with more people and landscapes, has become an ongoing trend in smartphones. However, all wide-angle images are suffering from perspective distortion, the straight lines appearing at the edges of the image will be curved, and the human faces will be unnatural, as shown in Fig. 1 (a).

To solve these problems, some classic calibration-based methods (Pavić, Schönefeld, and Kobbelt 2006; Carroll, Agarwala, and Agrawala 2010; Du, Hu, and Martin 2013; Tehrani, Majumder, and Gopi 2016) were proposed and the curved straight lines at the background can be corrected. But these conventional methods fail to correct the distorted faces, and even have a negative impact. Recent approaches (Shih et al. 2019; Tan et al. 2021) have considered to correct both distorted portraits and lines simultaneously. Especially, the first supervised CNN-based method was proposed by Tan et al. (Tan et al. 2021) and obtained satisfac-

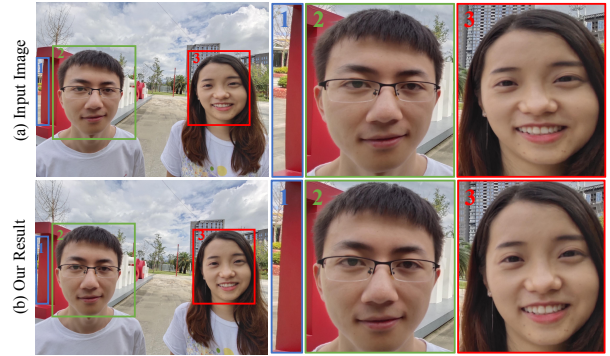


Figure 1: An example of our method. (a) the original wide-angle image with curved lines and distorted faces. (b) result by the proposed semi-supervised method, both lines and faces are corrected.

tory result. In Tan’s method, two networks were designed to remove the distortion on background and portraits respectively, achieving smooth transitions between perspective-rectified background and stereographic-rectified faces. Since there is no suitable dataset for training, they built a high-quality dataset over 5,000 labeled training samples. Nevertheless, there are still some drawbacks that restrict the continued ascension in their work. First, a well-generalized network needs a large amount of training data with rich types. The high cost makes it unrealistic to enlarge the labeled dataset. Second, in their two-stage network, the lines at the background are required to be corrected before processing the faces, causing the existence of redundancy. Third, although CNNs have achieved excellent performance, they always rely on the receptive fields and can’t learn long-range semantic information interaction well due to the locality of convolution operation.

Motivated by the above drawbacks, we attempt to leverage the unlabeled images to train a transformer-based network for wide-angle portraits correction. To be specific, we develop a novel network, dubbed as Multi-Scale Swin-Unet (MS-Unet), which is established based on the multi-scale swin transformer block (MSTB) to learn both local-scale and long-range information. Instead of two-stage learning

\*These authors contributed equally.

†Corresponding author

scheme (Tan et al. 2021), the MS-Unet can learn the correction flow maps from distortion image to normal image directly. Furthermore, we build a semi-supervised strategy, containing DRC and RC, to make full use of both labeled and unlabeled data by introducing a surrogate task (segmentation) in MS-Unet. In order to verify the effectiveness of the semi-supervised scheme, we collect more than 5,000 unlabeled distortion images from different phones and shooting scenes. By conducting sufficient experiments, we demonstrate the superior performance of our proposed method. Fig. 1 (b) shows our visual result.

In summary, our main contributions are:

- To the best of our knowledge, we propose the first semi-supervised learning strategy for wide-angle portraits correction, which dramatically reduces the requirement of labeled training data.
- We develop a novel transformer-based network called MS-Unet, based on MSTB, to fully utilize both local-scale and long-range semantic information interaction.
- We provide a high-quality unlabeled dataset that can be used for semi-supervised wide-angle portraits correction.

## 2 Related Works

### 2.1 Wide-Angle Portraits Correction

Early wide-angle portraits correction methods always relied on traditional algorithms. For example, stereographic projection (Svardal, Olsen, and Andersen 2003) can get very natural portraits, but the lines at the background are curved. Shih et al. (Shih et al. 2019) proposed a mesh-based algorithm that can strike a balance between straight lines and portraits correction effects. Nevertheless, it requires the camera parameters and portraits segmentation as input, leading complicated procedures. Recently, Tan et al. (Tan et al. 2021) proposed a two-stage deep neural network to complete wide-angle portraits correction, which solved the problem without camera parameters and portraits segmentation. Unfortunately, this fully supervised method is limited to the number of labeled data that requires high-cost manual screening and processing. Considering above reasons, we propose a semi-supervised transformer method, which can expand a large amount of training data at low cost, and effectively improve the effect of portraits correction.

### 2.2 Visual Transformer

The proposal of transformer (Vaswani et al. 2017) has been widespread used in natural language processing (NLP). Inspired by their outstanding achievements, researchers have gradually applied transformers to the computer vision field recently (Han et al. 2020; Khan et al. 2021). More impressively, Liu et al. (Liu et al. 2021) proposed an excellent hierarchical transformer structure called Swin Transformer, which is established upon shifted window partitioning mechanism. It has gained advanced performance on various vision tasks including image classification, object detection, and semantic segmentation. Hu et al. (Cao et al. 2021) also devised a U-shaped transformer block called Swin-Unet, which focused on the medical image segmentation and

achieved great results. Based on these works, we specially propose a new transformer network that is suitable for wide-angle portraits correction.

### 2.3 Deep Semi-Supervised Learning

Deep semi-supervised learning provides a practical and effective approach to fully utilize the mixture dataset containing labeled and unlabeled images. It has been widely used in image classification (Xu et al. 2017; Xie et al. 2020), semantic segmentation (Xiao et al. 2018; Babakhin, Sanakoyeu, and Kitamura 2019), machine translation (He et al. 2016; Cheng 2019), crowd counting (Liu et al. 2020; Meng et al. 2021), text classification (Karamanolakis, Hsu, and Gravano 2019; Li et al. 2019; Lee, Ko, and Han 2021) and so on. These works have proved that the semi-supervised learning can really promote the accuracy of network. Therefore, we also propose a semi-supervised learning method to break the constraint of the amount of labeled data in wide-angle portraits correction.

## 3 Method

In this section, we introduce the semi-supervised transformer for wide-angle portraits correction. Built upon Swin-Unet (Cao et al. 2021), we construct a network called Multi-Scale Swin-Unet (MS-Unet), which contains four major parts: encoder, bottleneck, decoder and skip fusion blocks. As shown in Fig. 2 (a), the network takes a single distortion image as input, and produces horizontal and vertical correction flow maps as intermediate outputs. Then the distortion image is projected into a normal image by the maps. Furthermore, we train our proposed MS-Unet through a semi-supervised scheme, which is achieved by direction and range consistency (DRC), and regression consistency (RC). The diagram of the semi-supervised is illustrated in Fig. 3.

### 3.1 Multi-Scale Swin-Unet (MS-Unet)

**Architecture Overview.** Our fundamental idea is to introduce the local-scale information into transformers, so that the features with local-scale and long-range information can be produced for accurate wide-angle portraits correction. Hence, we develop the MS-Unet, which is derived from Swin-Unet (Cao et al. 2021), to solve the above problems. As shown in Fig. 2 (a), the MS-Unet is divided into four major parts: encoder, decoder, bottleneck and skip fusion blocks.

For the encoder, the input with the size of  $H \times W$  is split into non-overlapping patches with size of  $4 \times 4$ . Then a linear embedding block is adopted on these patches to form the features with dimension  $C$ . In addition, there are four hierarchical stages in encoder and bottleneck, and each of them mainly contains two successive MSTBs and a patch merging block. Specially, the patch merging block is responsible for increasing dimension and down-sampling, while the MSTB is designed for local-scale and long-range information extraction. Inspired by U-Net (Ronneberger, Fischer, and Brox 2015), a symmetric architecture is deployed as the decoder. Contrary to the encoder, the decoder adopts patch expanding block for up-sampling and only a MSTB in each stage.

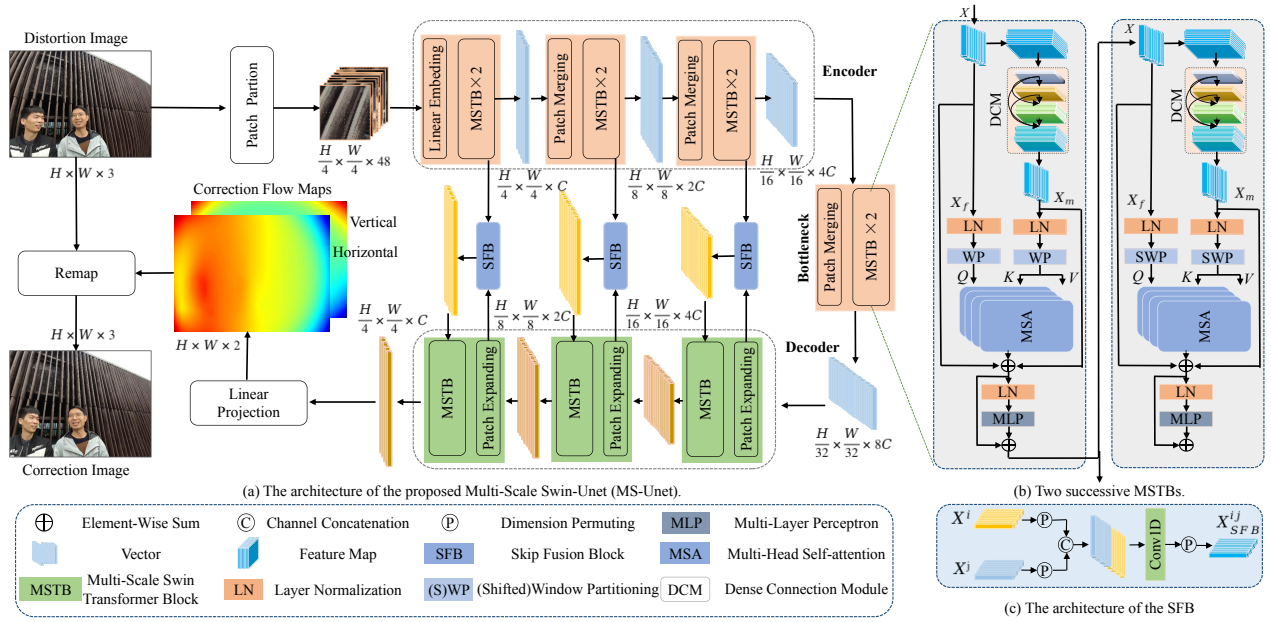


Figure 2: (a) The overview of our proposed Multi-Scale Swin-Unet (MS-Unet), which is built upon the multi-scale swin transformer block (MSTB). The network mainly consists of encoder, decoder, bottleneck and skip fusion blocks (SFB). (b) The architecture of two successive MSTBs. The primary difference between them is the windowing configurations (window partition and shifted window partition). (c) The detailed architecture of SFB.

Note that the outputs of each stage are fused with shallow features from encoder via the SFB before they are fed into next stage. Thus the missing spatial information caused by down-sampling will be complemented. Eventually, the final output features from the decoder share the same resolution with the input, and a linear projection layer is employed to produce the horizontal and vertical correction flow maps.

Overall, there are two primary differences between MS-Unet and Swin-Unet. First, as the core unit of Swin-Unet, swin transformer block ignores the importance of local-scale information, which leads that some objects (e.g., faces with different size) are still distorted after correction. Second, directly employing the skip connection may be not the optimal scheme for hierarchical features fusion owing to their difference. To alleviate these issues, we leverage the MSTB as the basic unit of our MS-Unet to integrate local-scale and long-range information. Furthermore, the simple yet efficient SFB is designed to replace the skip connection.

**Multi-Scale Swin-Transformer Block (MSTB).** We develop the dense connection module (DCM) into the MSTB for local multi-scale information extraction. In Fig. 2 (b), two successive MSTBs are presented. Each MSTB contains DCM, layernorm (LN), multi-head self-attention (MSA), skip connection, and multi-layer perceptron (MLP). The window partitioning (WP) and shifted window partitioning (SWP) are used in two successive MSTBs, respectively.

When the features  $X \in \mathbb{R}^{C \times H \times W}$  with a height of  $H$  and a width of  $W$  are fed into the MSTB, they will pass through two parallel branches for computing the query  $Q$ , key  $K$ , and value  $V$  as the input of MSA. In the left

branch,  $X$  are split into non-overlapping windows with size of  $h \times w$  by (S)WP. The features are flattened and reshaped as  $X_f \in \mathbb{R}^{N \times C}$ , where  $N = h \times w$ . Then a full connection layer is applied to obtain query  $Q \in \mathbb{R}^{N \times d}$ , where  $d = C/k$  and  $k$  is the head number. In the right branch, the features  $X$  are first utilized to extract local-scale information by DCM. Inspired by (Huang et al. 2017), the DCM consists of two  $1 \times 1$  layers, and three  $3 \times 3$  depthwise separable convolution layers with different dilation rates  $D = (1, 2, 3)$ . To be specific, the  $1 \times 1$  convolution layers are employed to change the feature dimension. Each  $3 \times 3$  depthwise separable convolution layer will receive the features from all preceding layers (i.e.,  $x_0, \dots, x_{r-1}$ ) as input:

$$x_r = C_r([x_0, \dots, x_{r-1}]) \quad (1)$$

where  $C_r$  denotes the concatenation operation. Then we apply the same operations like the left branch on these features from the DCM to generate  $X_m \in \mathbb{R}^{N \times C}$ . The key  $K \in \mathbb{R}^{N \times d}$ , and value  $V \in \mathbb{R}^{N \times d}$  are obtained through  $X_m$ . Afterwards, the MSA can be calculated as follows:

$$MSA(Q, K, V) = \text{Softmax}\left(\frac{QK^T}{\sqrt{d}} + B\right)V \quad (2)$$

where  $B \in \mathbb{R}^{N \times N}$  refers to learnable relative position bias.

**Skip Fusion Block (SFB).** As mentioned above, the crucial difference among features from different hierarchical stages will be ignored when directly adopting skip connection. Hence, we specifically design the simple yet efficient skip fusion block (SFB) to replace the skip connection. As shown in Fig. 2 (c), before the features  $X^i \in \mathbb{R}^{N \times C}$ ,  $X^j \in \mathbb{R}^{N \times C}$  (from the  $i^{th}$  stage of encoder, and the  $j^{th}$



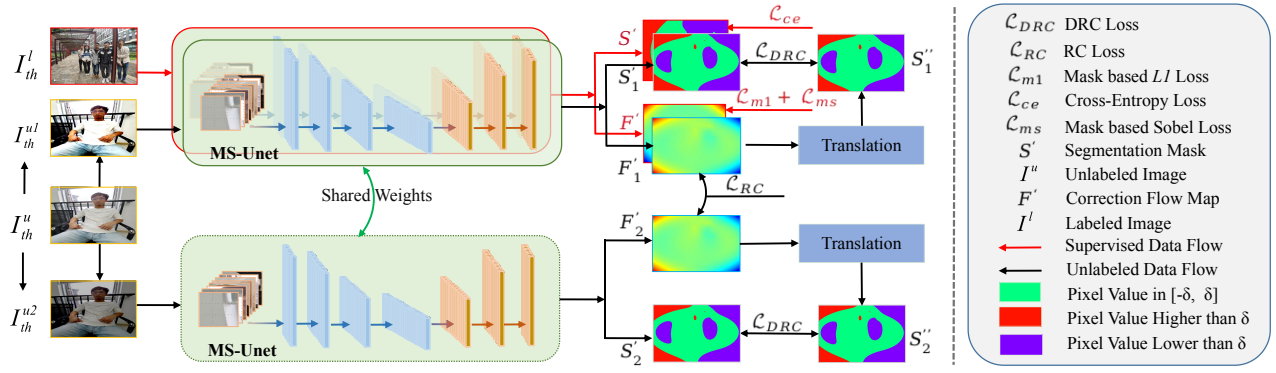


Figure 3: The pipeline of semi-supervised wide-angle portraits correction framework, which consists of direction and range consistency (DRC), regression consistency (RC). For an unlabeled image  $I_{th}^u$ , when it is sent to the siamese network, the estimated segmentation mask and correction mask are utilized to compute the  $\mathcal{L}_{DRC}$  and  $\mathcal{L}_{RC}$  using unsupervised loss. The unlabeled data flow is marked with black. In addition, the labeled data flow marked with red is also illustrated.

stage of decoder) are sent to the next stage of decoder, they pass through the SFB to form new features  $X_{SFB}^{ij}$  with dimension  $\mathbb{R}^{N \times C}$ . The whole calculation process is defined as follows:

$$X_{SFB}^{ij} = D(CON(C[D(X^i), D(X^j)])) \quad (3)$$

where  $D(\cdot)$  is dimension permuting,  $C[\cdot]$  refers to the concatenation, and  $CON(\cdot)$  is 1D convolution layer.

### 3.2 Semi-supervised Learning Algorithm

Although the MS-Unet can boost the performance significantly, training a superior portraits correction network is really dependent on the high-quality labeled data. However, obtaining the labeled data is not easy owing to the extremely high cost. To reduce the cost of labeling, we train our proposed MS-Unet through a semi-supervised scheme, which allows us to use fewer labeled images to obtain better effect. In our problem settings, we have a set of unlabeled images noted as  $U = (I_{th}^u)$  and a set of labeled images  $L = (I_{th}^l, F_{th})$ , where  $F_{th}$  represents the labels. We mix these images and adopt them to train our network through the semi-supervised method composed of DRC and RC.

**Direction and Range Consistency (DRC).** Many existing methods have proved that a network performance can be further improved by introducing approximate surrogate tasks (Gao, Wang, and Li 2019; Meng et al. 2021). Thus we construct a surrogate task (segmentation) in the MS-Unet to predict whether the flow map value,  $F(i, j)$ , meets the given direction and range. To be specific, the prediction target of the segmentation task is defined as follows:

$$S(i, j) = \begin{cases} 0, & \text{if } F(i, j) \leq -\delta \\ 1, & \text{if } -\delta < F(i, j) < \delta \\ 2, & \text{if } F(i, j) \geq \delta \end{cases} \quad (4)$$

where  $S(i, j)$  denotes the segmentation mask,  $(i, j)$  is the pixel position of mask or flow map, and  $\delta$  is the predefined threshold, which is set to 5 in our experiments.

This design is mainly motivated by four aspects: 1) Each pixel on the correction flow map is directional. The network

can learn the direction variation of each pixel through segmentation mask, which is beneficial to get a better understanding of portraits correction. 2) By expressing a variation range with the same threshold, the segmentation mask can make the network learn regional consistency, so that the estimated correction flow maps will become smoother. 3) The ground truth segmentation mask can be generated directly by using the existing correction labels without additional cost. 4) The loss function can be constructed between portraits correction and segmentation, which makes it feasible to introduce unlabeled data by our semi-supervised scheme.

The learning strategy of DRC is shown in Fig. 3. For labeled data, the segmentation task is supervised through the label transformed from ground truth flow map. For the unlabeled images, they are utilized by the network to learn direction and range consistency. We will give the details of semi-supervised loss in section 3.3.

**Regression Consistency(RC).** Besides the DRC, we also introduce the regression consistency (RC) to improve the network robustness. Fig. 3 illustrates the details of RC. Specifically, we can obtain two different images  $I_{th}^{u1}$  and  $I_{th}^{u2}$  with various augmentation methods (e.g., noise, smoothing, and sharpening), from an unlabeled image  $I_{th}^u$ . Many previous works have stated that when an image with different perturbations, the same predictions can be obtained through the same network, which means that an excellent network is robust. Therefore, we expand the MS-Unet into a shared-weight siamese structure. The unlabeled images  $I_{th}^{u1}$  and  $I_{th}^{u2}$  are respectively fed into the two networks and a consistent loss is established between their outputs. The detailed loss implementation of RC will be given in section 3.3.

### 3.3 Loss Function

In practice, the MS-Unet is optimized by adopting the supervised losses (flow map regression, and segmentation task) on the labeled data  $L$ , and the semi-supervised losses on the unlabeled data  $U$ .



**Supervised Loss.** Our constructed supervised loss  $\mathcal{L}_s$  is composed of three parts, including mask-based L1 loss  $\mathcal{L}_{m1}$ , mask-based sobel loss  $\mathcal{L}_{ms}$ , and the cross-entropy loss  $\mathcal{L}_{ce}$ . The detailed definitions are described as follows:

a)  $\mathcal{L}_{m1}$  Loss: In our method, we introduce the weighted mask, where the weight value in portrait region is always larger than background. Thus the network will pay more attention to distortion portraits. Eq. 5 gives the definition of this loss.

$$\mathcal{L}_{m1} = |F' - F| M \quad (5)$$

where  $F$  and  $F'$  represent the ground truth and estimated flow maps, respectively,  $M$  denotes the weighted mask.

b)  $\mathcal{L}_{ms}$  Loss: In portraits correction, the object edges directly affect the overall visual effects of a correction image. Therefore, we introduce the sobel loss which can be expressed as follows:

$$\mathcal{L}_{ms} = [|G_x(F') - G_x(F)| + |G_y(F') - G_y(F)|] M \quad (6)$$

where the  $G_x$  and  $G_y$  mean the horizontal and vertical sobel kernel, respectively.

c)  $\mathcal{L}_{ce}$  Loss: To supervise the mask generated from the segmentation task, we convert the ground truth flow map into mask label and deploy the cross-entropy loss. The loss function is defined as follows:

$$\mathcal{L}_{ce} = S \log(S') + (1 - S) \log(1 - S') \quad (7)$$

where the  $S$  is the ground truth mask converted from the flow map, and the  $S'$  refer to the estimated mask. To sum up, the training loss for a labeled image is:

$$\mathcal{L}_s = \mathcal{L}_{m1} + \lambda_1 \mathcal{L}_{ms} + \lambda_2 \mathcal{L}_{ce} \quad (8)$$

where  $\lambda_1$  and  $\lambda_2$  are hyper-parameters, both being set to 10 in our experiments.

**Semi-Supervised Loss.** For an unlabeled image, we construct the unsupervised loss  $\mathcal{L}_u$  based on segmentation task and flow map task to guide the prediction consistency of the network. The unsupervised loss contains two parts: the loss of DRC  $\mathcal{L}_{DRC}$  and RC  $\mathcal{L}_{RC}$ .

$$\begin{aligned} \mathcal{L}_u &= \mathcal{L}_{RC} + \mathcal{L}_{DRC} \\ &= [\mathcal{L}_{m1}(F'_1, F'_2) + \lambda_2 \mathcal{L}_{ms}(F'_1, F'_2)] + \\ &\quad [\mathcal{L}_{ce}(S'_1, S''_1) + \mathcal{L}_{ce}(S'_2, S''_2)] \end{aligned} \quad (9)$$

where the  $F'_1$  and  $F'_2$  are the estimated flow maps from both the branches of the siamese network,  $S'_1$  and  $S'_2$  refer to the segmentation mask converted from  $F'_1$  and  $F'_2$ , while the  $S''_1$  and  $S''_2$  indicate the output of the siamese network.

## 4 Experiments

### 4.1 Implementation Details

**Datasets.** Following the existing method (Tan et al. 2021), we conduct extensive experiments on the wide-angle dataset (Tan et al. 2021), captured from 5 different smartphones. The dataset consists of over 5,000 images in the training set, and 129 images in the testing set. For each image in the dataset, many kinds of labels are provided, containing the face mask, correction flow maps, and landmarks. In addition, we collect another more than 5,000 images through 4 different smartphones (including Samsung Note 10, Xiaomi 11, vivo X23 and vivo iQOO) as the unlabeled set.

**Training Details.** In the training stage, we train the MS-Unet via a two-step scheduling scheme. In the first stage, we only train correction flow map predictor until 200 epochs. Then, we introduce the surrogate task and the semi-supervised method to further improve the performance of the network. In this stage, the total training epoch is set to 1,000 in our experiments. For both steps, we use Adam to optimize our model with a initial learning rate of  $1 \times 10^{-4}$ , and the weight decay of  $2 \times 10^{-4}$ . In addition, we adopt some data enhancement methods (e.g., zooming, sharpening, smoothing) to enrich the diversity of training samples. All the experiments are performed with 4 Geforce RTX 2080Ti.

**Evaluation Metrics.** We use the same evaluation metrics (LineAcc and ShapeAcc) as (Tan et al. 2021) to evaluate the performance of our proposed method. More specifically, LineAcc is used to evaluate the curvature variation of the marked lines and defined as follows:

$$LS = 1 - \frac{1}{n} \sum_{i=0}^{n-1} \left( \frac{y_{d_i} - y_{d_{i-1}}}{x_{d_i} - x_{d_{i-1}}} - \frac{y_{g_0} - y_{g_n}}{x_{g_0} - x_{g_n}} \right) \quad (10)$$

where  $LS$  denotes the similarity between slope of these two lines,  $n$  is the number of uniformly sampled points in each line.  $(x_{g_i}, y_{g_i})$  and  $(x_{d_i}, y_{d_i})$  indicate the coordinate of the corresponding point in the reference and distortion image.

ShapeAcc aims to evaluate the face similarity between the correction image and the reference image. Based on face landmarks, the ShapeAcc is described as follows:

$$FC = \frac{1}{n} \sum_{i=0}^{n-1} \|L_{g_i}\| \|L_{d_i}\| \cos\theta \quad (11)$$

where  $FC$  is the similarity between the corrected and target face,  $n$  is the number of fixed sampled points in each face.  $L_g$  and  $L_d$  are the corresponding face landmarks in the correction image and the reference image.

### 4.2 Ablation Study

In order to verify the influence of different factors on our proposed method, we conduct some ablation experiments on Tan's dataset (Tan et al. 2021) and our unlabeled dataset. In particular, the structure of correction network, the semi-supervised strategy, and the number of unlabeled samples are all considered below.

**Effect of the Correction Network.** We first explore that how the proposed modules (i.e., MSTB, SFB) affect the network performance. To be specific, we utilize the Swin-Unet as our baseline, and the performance of three different networks are evaluated. 1) Baseline: directly employ the Swin-Unet to predict correction flow maps; 2) Baseline+MSTB: based on 1), the MSTB is considered to replace the swin transformer block for integrating local-scale information; 3) Baseline+MSTB+SFB (MS-Unet): the SFB is added to effectively fuse the hierarchical features. Table 1 presents the results of the experiments. From it we can observe that the performance boosts significantly with the addition of each module. Especially, when both MSTB and SFB are added to the network, the full MS-Unet can achieve the best LineAcc (66.825) and ShapeAcc (97.491). These experiments



Figure 4: Qualitative results of different wide-angle portraits correction methods.

demonstrate that MSTB indeed promotes the network to extract more complementary information, which boosts the correction ability dramatically. Meanwhile, SFB provides a better feature fusion strategy than skip connections.

Table 1: Ablations on the structure of proposed MS-Unet.

Index	Baseline	MSTB	SFB	LineAcc	ShapeAcc
1)	✓	-	-	66.514	97.460
2)	✓	✓	-	66.763	97.487
3)	✓	✓	✓	<b>66.825</b>	<b>97.491</b>

**Effect of the Semi-Supervised Strategy.** Several experiments are conducted to evaluate the impact of our proposed semi-supervised scheme. Both labeled and unlabeled data are deployed to accomplish our experiments. In each experiment, the network is trained using supervised scheme for 200 epochs before the semi-strategy is deployed, and then the network will remain to be trained for 1,000 epochs.

We first simply add the surrogate task (segmentation) to the network and continue to train the two-task MS-Unet without any unlabeled images. The second row in Table 2 reports the results of the two-task MS-Unet. Compared with the MS-Unet with only correction task, it shows a slight improvement after adding the surrogate task (LineAcc: 66.825  $\rightarrow$  66.871, ShapeAcc: 97.491  $\rightarrow$  97.493). This indicates that the learning ability of MS-Unet can be further improved via segmentation task. Then the DRC is conducted based on the segmentation task, and the third row in Table 2 lists the comparison result. Compared with the two-task MS-Unet, adding DRC can further improve the estimation accuracy of the correction flow maps, especially the LineAcc (from 66.871 to 67.154). Besides, the effect of RC is also evaluated and the result is presented in the fourth row of Table 2. The result also outperforms the single-task MS-Unet, which is only trained by supervised scheme. From

all the list, the MS-Unet attains the best result (LineAcc: 67.209, ShapeAcc: 97.500) when both DRC and RC are employed during the semi-supervised training.

Table 2: Performance comparison of different semi-supervised strategies. 'Seg' indicates a segmentation task without direction and range consistency.

Index	Seg	DRC	RC	LineAcc	ShapAcc
1)	-	-	-	66.825	97.491
2)	✓	-	-	66.871	97.493
3)	✓	✓	-	67.154	97.494
4)	-	-	✓	66.848	97.497
5)	✓	✓	✓	<b>67.209</b>	<b>97.500</b>

**Effect of the Number of Unlabeled Samples.** We examine the influence of the number of unlabeled images on network performance through Tan's dataset (Tan et al. 2021) and our unlabeled data. We change the amount of unlabeled images from 0 to 5,000 while the number of labeled images are fixed. The results are listed in Table 3, where it shows our MS-Unet trained with semi-supervised strategy obtains consistent superior performance compared with that using the fully-supervised scheme. Meanwhile, we can draw that in a certain range, the performance of the MS-Unet will improve as the amount of unlabeled images increases.

Table 3: The impact of the number of unlabeled images.

Index	numbers	LineAcc	ShapeAcc
1)	0	66.871	97.493
2)	1000	66.929	97.493
3)	2000	66.999	97.494
4)	3000	67.105	97.497
5)	4000	67.155	97.496
6)	5000	<b>67.209</b>	<b>97.500</b>

### 4.3 Comparison with Other Methods

**Comparison with Other Wide-Angle Portraits Correction Methods.** We also compare our proposed method with previous state-of-the-art methods on Tan’s and Google’s test sets. Table 4 illustrates that our method obtains the highest metric results in both two test sets. The visual comparisons in Fig. 8 also confirm the metric results. Note that the projection image can correct lines but make faces distorted seriously. Shih (Shih et al. 2019) and Tan (Tan et al. 2021) try to seek the optimal trade-off between the faces and the background. Unfortunately, there still exists several bended structures at the background, and a few faces are still distorted. From our results, we can draw that the faces are more natural, and the corrected structures in the background are satisfactory. Both quantitative and qualitative results verify the superior performance of our method.

Table 4: Quantitative results on two wide-angle portraits correction test sets.

Method	Tan’s test set		Google’s test set	
	LineAcc	ShapeAcc	LineAcc	ShapeAcc
Shih(Shih et al. 2019)	66.143	97.253	61.551	97.464
Tan(Tan et al. 2021)	66.784	97.490	64.650	97.499
Ours	<b>67.209</b>	<b>97.500</b>	<b>66.098</b>	<b>97.512</b>

Fig. 5 depicts the results of our method and other popular portraits correction algorithms from smartphones (i.e., Xiaomi 11 ultra, and iPhone 12). We can observe that serious stretching of portraits appear in iPhone 12. Although the result of Xiaomi 11 ultra improves than the distortion image, there are still slight deformation on the face and curved lines at the background. Our method shows better results, as the face is natural while correcting the lines at the background.

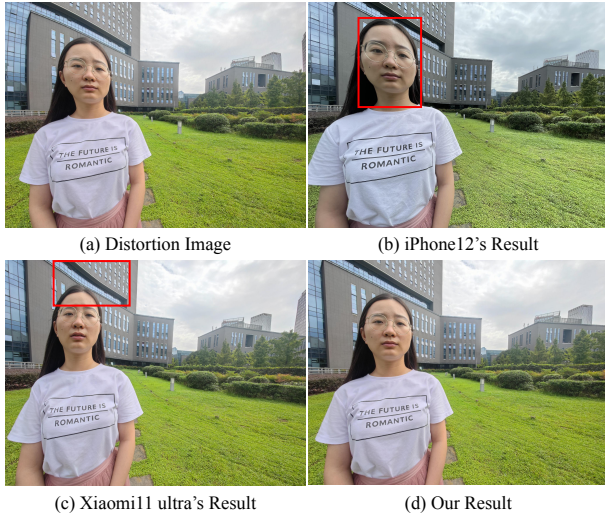


Figure 5: Visual comparison between our method and some wide-angle portraits correction methods from smartphones.

**Comparison with Other Computer Vision Methods.** At present, only few works employ the deep learning meth-

ods to implement wide-angle portraits correction due to its challenge. Based on the correction flow maps, the correction task is transformed into a pixel-level regression problem, which is closely related to some computer vision tasks, such as crowd counting (Gao, Wang, and Li 2019; Liu et al. 2020) and semantic segmentation(Chen et al. 2018; Cao et al. 2021). Hence, we introduce some efficient networks from these fields to predict the correction flow maps. All the networks are trained by full supervised scheme, and Table 5 shows the results. Notably, our proposed MS-Unet surpasses all the other methods. The primary reason is that the CNN-based networks focus on learning local-scale information while the transformer-based networks concentrate more on building long-range information. Combining both of their advantages, the MS-Unet will capture multi-scale information for more accurate estimation of correction flow maps.

Table 5: The results of different networks about wide-angle portraits correction.

Method	LineAcc	ShapeAcc
RefineNet(Lin et al. 2017)	66.348	97.449
CSRNet(Li and Zhang 2018)	65.967	97.469
Deeplab v3+(Chen et al. 2018)	66.200	97.482
Swin-Unet(Cao et al. 2021)	66.514	97.460
HRNet(Sun et al. 2019)	66.748	97.477
Ours	<b>66.825</b>	<b>97.491</b>

Besides, our semi-supervised method is employed to train these networks. The results in Table 6 demonstrate the generalization ability of our semi-supervised method.

Table 6: The effectiveness evaluation of the proposed semi-supervised scheme on different networks.

Method	Fully-Supervised		Semi-Supervised	
	LineAcc	ShapeAcc	LineAcc	ShapeAcc
RefineNet(Lin et al. 2017)	66.348	97.449	66.569	97.455
CSRNet (Li and Zhang 2018)	65.967	97.469	66.236	97.471
Deeplab v3+ (Chen et al. 2018)	66.200	97.482	66.565	97.487
Swin-Unet(Cao et al. 2021)	66.514	97.460	66.859	97.469
HRNet(Sun et al. 2019)	66.748	97.477	66.805	97.491
Ours	<b>66.825</b>	<b>97.491</b>	<b>67.209</b>	<b>97.500</b>

## 5 Conclusion

In this paper, we develop a novel semi-supervised wide-angle portraits correction method using multi-scale transformer. In order to capture both local-scale and long-range information, we design the MS-Unet, which takes the MSTB as the core unit. We also design the SFB and add it to our network for integrating hierarchical features effectively. Furthermore, we develop a semi-supervised manner to train our network. By combining DRC and RC, we can solve the limitations of labeled data and make full use of unlabeled data. In addition, four kinds of smartphones are adopted to collect available unlabeled data. Extensive experimental results show that our proposed method is much better than the existing advanced methods, and has the ability to be popularized in the application of wide-angle portraits correction.



## References

- Babakhin, Y.; Sanakoyeu, A.; and Kitamura, H. 2019. Semi-supervised segmentation of salt bodies in seismic images using an ensemble of convolutional neural networks. In *German Conference on Pattern Recognition*, 218–231. [2](#)
- Cao, H.; Wang, Y.; Chen, J.; Jiang, D.; Zhang, X.; Tian, Q.; and Wang, M. 2021. Swin-Unet: Unet-like Pure Transformer for Medical Image Segmentation. *arXiv preprint arXiv:2105.05537*. [2](#), [7](#)
- Carroll, R.; Agarwala, A.; and Agrawala, M. 2010. Image warps for artistic perspective manipulation. *ACM Trans. Graphics*, 29(4): 1–9. [1](#)
- Chen, L.-C.; Zhu, Y.; Papandreou, G.; Schroff, F.; and Adam, H. 2018. Encoder-decoder with atrous separable convolution for semantic image segmentation. In *Proc. ECCV*, 801–818. [7](#)
- Cheng, Y. 2019. Semi-supervised learning for neural machine translation. In *Joint training for neural machine translation*, 25–40. [2](#)
- Du, S.-P.; Hu, S.-M.; and Martin, R. R. 2013. Changing perspective in stereoscopic images. *IEEE Trans. on Visualization and Computer Graphics*, 19(8): 1288–1297. [1](#)
- Gao, J.; Wang, Q.; and Li, X. 2019. Pcc net: Perspective crowd counting via spatial convolutional network. *IEEE Trans. on Circuits and Systems for Video Technology*, 30(10): 3486–3498. [4](#), [7](#)
- Han, K.; Wang, Y.; Chen, H.; Chen, X.; Guo, J.; Liu, Z.; Tang, Y.; Xiao, A.; Xu, C.; Xu, Y.; et al. 2020. A survey on visual transformer. *arXiv preprint arXiv:2012.12556*. [2](#)
- He, D.; Xia, Y.; Qin, T.; Wang, L.; Yu, N.; Liu, T.-Y.; and Ma, W.-Y. 2016. Dual learning for machine translation. *Proc. NeurIPS*, 29: 820–828. [2](#)
- Huang, G.; Liu, Z.; Van Der Maaten, L.; and Weinberger, K. Q. 2017. Densely connected convolutional networks. In *Proc. CVPR*, 4700–4708. [3](#)
- Karamanolakis, G.; Hsu, D.; and Gravano, L. 2019. Leveraging just a few keywords for fine-grained aspect detection through weakly supervised co-training. *arXiv preprint arXiv:1909.00415*. [2](#)
- Khan, S.; Naseer, M.; Hayat, M.; Zamir, S. W.; Khan, F.; and Shah, M. 2021. Transformers in Vision: A Survey. *ArXiv*, abs/2101.01169. [2](#)
- Lee, J.-H.; Ko, S.-K.; and Han, Y.-S. 2021. SALNet: Semi-supervised Few-Shot Text Classification with Attention-based Lexicon Construction. In *Proc. AAAI*, 13189–13197. [2](#)
- Li, X.; Sun, Q.; Liu, Y.; Zhou, Q.; Zheng, S.; Chua, T.-S.; and Schiele, B. 2019. Learning to self-train for semi-supervised few-shot classification. *Proc. NeurIPS*, 32: 10276–10286. [2](#)
- Li, Y.; and Zhang, X. 2018. Csrnet: Dilated convolutional neural networks for understanding the highly congested scenes. In *Proc. CVPR*, 1091–1100. [7](#)
- Lin, G.; Milan, A.; Shen, C.; and Reid, I. 2017. Refinenet: Multi-path refinement networks for high-resolution semantic segmentation. In *Proc. CVPR*, 1925–1934. [7](#)
- Liu, Y.; Liu, L.; Wang, P.; Zhang, P.; and Lei, Y. 2020. Semi-supervised crowd counting via self-training on surrogate tasks. In *Proc. ECCV*, 242–259. [2](#), [7](#)
- Liu, Z.; Lin, Y.; Cao, Y.; Hu, H.; Wei, Y.; Zhang, Z.; Lin, S.; and Guo, B. 2021. Swin transformer: Hierarchical vision transformer using shifted windows. *arXiv preprint arXiv:2103.14030*. [2](#)
- Meng, Y.; Zhang, H.; Zhao, Y.; Yang, X.; Qian, X.; Huang, X.; and Zheng, Y. 2021. Spatial Uncertainty-Aware Semi-Supervised Crowd Counting. *arXiv preprint arXiv:2107.13271*. [2](#), [4](#)
- Pavić, D.; Schönefeld, V.; and Kobbelt, L. 2006. Interactive image completion with perspective correction. *The Visual Computer*, 22(9-11): 671–681. [1](#)
- Ronneberger, O.; Fischer, P.; and Brox, T. 2015. U-net: Convolutional networks for biomedical image segmentation. In *International Conference on Medical image computing and computer-assisted intervention*, 234–241. [2](#)
- Shih, Y.; Lai, W.-S.; Liang, C.-K.; and Liang, C.-K. 2019. Distortion-free wide-angle portraits on camera phones. *ACM Trans. Graphics*, 38(4): 1–12. [1](#), [2](#), [7](#), [9](#)
- Sun, K.; Xiao, B.; Liu, D.; and Wang, J. 2019. Deep high-resolution representation learning for human pose estimation. In *Proc. CVPR*, 5693–5703. [7](#)
- Svardal, B. S.; Olsen, K. E.; and Andersen, O. R. 2003. Stereographic projection system. US Patent 6,547,396. [2](#)
- Tan, J.; Zhao, S.; Xiong, P.; Liu, J.; Fan, H.; and Liu, S. 2021. Practical Wide-Angle Portraits Correction with Deep Structured Models. In *Proc. CVPR*, 3498–3506. [1](#), [2](#), [5](#), [6](#), [7](#), [9](#)
- Tehrani, M. A.; Majumder, A.; and Gopi, M. 2016. Correcting perceived perspective distortions using object specific planar transformations. In *Proc. ICCP*, 1–10. [1](#)
- Vaswani, A.; Shazeer, N.; Parmar, N.; Uszkoreit, J.; Jones, L.; Gomez, A. N.; Kaiser, Ł.; and Polosukhin, I. 2017. Attention is all you need. In *Proc. NeurIPS*, 5998–6008. [2](#)
- Xiao, H.; Wei, Y.; Liu, Y.; Zhang, M.; and Feng, J. 2018. Transferable semi-supervised semantic segmentation. In *Proc. AAAI*. [2](#)
- Xie, Q.; Luong, M.-T.; Hovy, E.; and Le, Q. V. 2020. Self-training with noisy student improves imagenet classification. In *Proc. CVPR*, 10687–10698. [2](#)
- Xu, W.; Sun, H.; Deng, C.; and Tan, Y. 2017. Variational autoencoder for semi-supervised text classification. *Proc. AAAI*. [2](#)

## A Additional Implementation Details

### A.1 Image Scaling

In our experiments, the original distortion images from smartphones are not straight-forward for training directly due to the large size. Therefore, we scale all the images to a uniform size with  $384 \times 512$ , and send the resized images to our MS-Unet for training. Consequently, the the output correction flow maps share the same size (i.e.,  $384 \times 512$ ) with the resized images. Afterwards, the correction flow maps are resized as the same size as the original images, and then they are utilized to correct the original distortion images into normal images. This scaling policy enables our MS-Unet to be executed under a lower complexity, which makes it feasible to apply into smartphones.

### A.2 Correction Flow Map & Segmentation Mask

In Tan’s method (Tan et al. 2021), two sub-networks were designed to implement the wide-angle portraits correction. In their method, the LineNet produces the perspective projection flow maps to project the distortion image as flattened, while the ShapeNet predicts the face correction flow maps to correct the flattened images into normal images. To reduce the structural redundancy, we design the one-stage network called MS-Unet to generate the correction flow maps, which can project the distortion image into normal image directly.

Fig. 6 shows some corrected images by our MS-Unet, as well as the corresponding correction flow maps (including horizontal and vertical correction flow maps). Usually the darker the region in the flow map, the stronger correction the region requires. Consequently, we can observe that the flow maps pay more attention to the distortion faces in addition to the corners of the distortion image. Meanwhile, Fig. 6 also illustrates the corresponding segmentation mask of each flow map, which is developed to assist our semi-supervised scheme.

## B Introduction about the Unlabeled Data

We construct the unlabeled dataset containing 5,000 distortion images with various scenes and smartphones. This dataset make it possible to train the MS-Unet with our proposed semi-supervised scheme.

Table 7 illustrates the specific distribution of our unlabeled data divided by the number of people and the orientation. The samples in the unlabeled dataset are captured with 4 types of smartphones (including Samsung Note 10, Xiaomi 11, vivo X23 and vivo iQOO) with wide-angle lens of different distortion modules. Each smartphone contains various scenes with both horizontal and vertical orientation, and the number of people in each image is also range from 1 to 3, corresponding to(Scene 1-H to Scene 3-V in Table 7). Meanwhile, we present the specific sample number of each scene, as well as its percentage over all dataset. Notably, the number of people is evenly distributed on both smartphones and scenes.

Besides, our unlabeled dataset contains a variety of complex scenes, and some samples are show in Fig. 7. To be specific, these images are captured with different shooting

ways. In particular, the shooting ways include different number of people, shooting angles and shooting distances, as shown in Fig. 7. Different shooting ways are combined with different orientation, covering various types of distortions.

## C Comparison Results

### C.1 Comparison with Other Methods

We show more visual comparisons with perspective undistortion, Shih’ results (Shih et al. 2019), and Tan’s results (Tan et al. 2021). We mark the obvious differences in the corrected images with red boxes. In general, our proposed method strikes a better balance between correcting the straight lines and distortion faces. Moreover, it keeps a more natural transition between the faces and the background.

### C.2 Comparison with Other Phones

In addition, Fig. 9 shows more visual results compared with the corrected wide-angle portraits images by iPhone 12 and Xiaomi 11. We can clearly observe that our proposed method is superior to the two commercial solutions. Especially the region marked with red box, the corrected faces is more natural than others.

### C.3 Our Future Research Direction

Although our proposed method can correct distortion images well in many scenes, the performance needs to be further improved in some scenes. As shown in Fig. 10, we further evaluate the effectiveness of our proposed method, and explore the space to further enhance. Fig. 10 (a) shows two unsatisfactory examples where the feet are close to the corners of the images. It is inevitable to force the feet to overstretch when correcting the corners. Similarly, the body in Fig. 10 (b) is also overstretch due to the strong correction of corners. The main reason is that the current ground truth flow maps only focus on the correction of distorted faces but ignore the other part of the body, such as feet and arms. In the future, we will continue to expand our work to correct the distortion of the whole body, which can solve the problem mentioned in Fig. 10. Also, it will make the corrected images more natural.

Table 7: Unlabeled dataset distribution on different camera modules with different number of people and orientations. 'H' indicates the image in horizontal orientation, and 'V' refers to the image in vertical orientation.

	Scene 1-H	Scene 1-V	Scene 2-H	Scene 2-V	Scene 3-H	Scene 3-V	Total
Xiaomi 11	226	194	229	224	198	189	1,260 (25.20%)
Samsung Note10	224	219	214	209	199	189	1,254 (25.08%)
vivo X23	231	195	198	238	211	196	1,269 (25.38%)
vivo iQOO	198	218	213	196	191	201	1,217 (24.34%)
Total	879(17.58%)	826(16.52%)	854(17.08%)	867(17.34%)	799(15.98%)	775(15.50%)	5,000

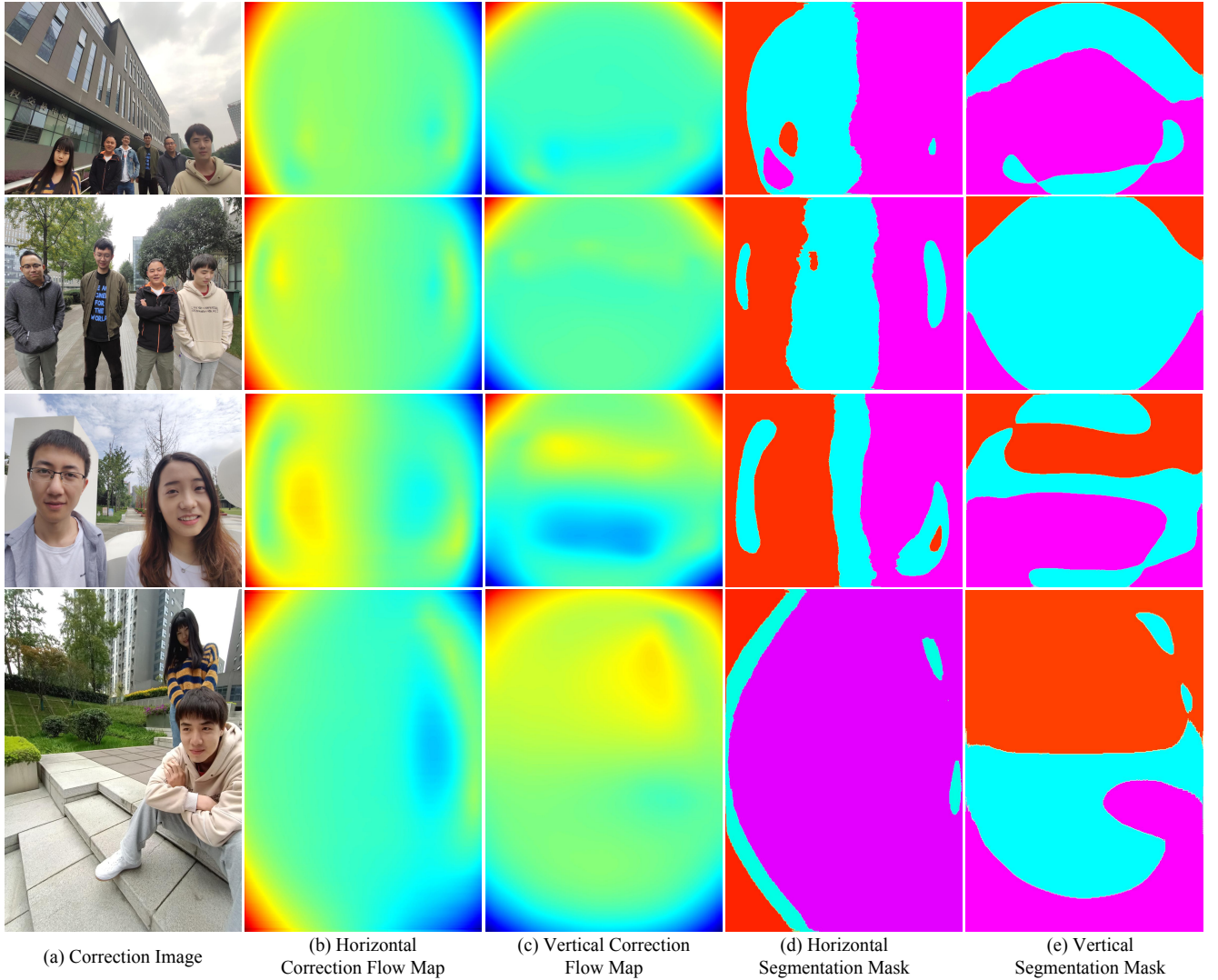


Figure 6: Visualization results of our proposed methods. From left to right: (a) the correction images, (b) the horizontal correction flow map, (c) the vertical correction flow map, (d) the horizontal segmentation mask, (e) the vertical segmentation mask.



(a) Scene 1



(b) Scene 2



(c) Scene 3



(d) Different Distances



(d) Different Angles



Figure 7: Some samples of different scenes in our unlabeled dataset. 5 different shooting scenes with various people and backgrounds are shown in this figure.





Figure 8: Qualitative results of different wide-angle portraits correction methods. Note that the obvious differences in the corrected images are marked with red boxes.





Figure 9: Visual comparison between our method and two other smartphones with wide-angle portraits correction methods. We mark the obvious differences in the correction images with red boxes.



Figure 10: Some corrected images that require to be further improved.